JCTC Journal of Chemical Theory and Computation

Article

pubs.acs.org/JCTC

Calculation of Lipid-Bilayer Permeabilities Using an Average Force

Jeffrey Comer,[†] Klaus Schulten,[‡,§] and Christophe Chipot*[,†,§]

[†]Laboratoire International Associé, Centre National de la Recherche Scientifique et University of Illinois at Urbana−Champaign, Unité Mixte de Recherche n°7565, Université de Lorraine, B.P. 70239 54506 Vandœuvre-lès-Nancy cedex, France

[‡]Department of Physics, University of Illinois at Urbana−Champaign, 1110 West Green Street, Urbana, Illinois 61801, United States

[§]Theoretical and Computational Biophysics Group, Beckman Institute for Advanced Science and Engineering, University of Illinois at Urbana−Champaign, 405 North Mathews, Urbana, Illinois 61801, United States

ABSTRACT: Calculations of lipid bilayer permeabilities from first principles, using molecular simulations, would be valuable to rapidly assess the bioavailability of drug candidates, as well as to decipher, at the atomic level, the mechanisms that underlie the translocation of permeants. The most common theoretical approach, the solubility−diffusion model, requires determination of the free energy and the diffusivity as functions of the position of the permeant. Quantitative predictions of permeability have, however, been stymied by acute difficulties in calculating the diffusivity, inadequate sampling, and, most insidiously, systematic biases due to imperfections in the force field, simulation parameters, and the inherent limitations of the diffusive model. In the present work, we combine importance-sampling simulations employing an adaptive biasing force with a Bayesian-inference algorithm to determine the free energy and diffusivity with noteworthy precision and spatial resolution. In multimicrosecond simulations, we probe the sensitivity of the permeability estimates to different aspects of the methodology, including the truncation of short-range interactions, the thermostat, the force-field parameters of the permeant, the time scale over which the diffusivity is estimated, and the size of the simulated system. The force-field parameters and time scale dependence of the diffusivities impose the greatest uncertainties on the permeability estimates. Our simulations highlight the importance of membrane distortion due to the presence of the permeant, which may be partially suppressed if the bilayer patch is not large enough. We suggest that improvements to force fields and more robust kinetic models may be needed to reduce systematic errors below a factor of two.

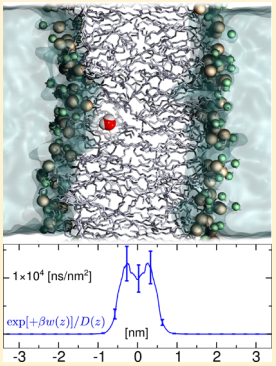

1. INTRODUCTION

In the development of new therapeutic agents, the concept of bioavailability is particularly crucial, dictating the natural propensity of the drug to overcome biological barriers, such as membranes, and reach its designated target in sufficient quantity. One of the longstanding challenges of the pharmaceutical industry has been to identify, as early as possible in the drug discovery process, potential failures of the candidate molecules to attain their target. In particular, it would be highly desirable to assess drug bioavailability before investing in expensive organic syntheses, let alone in prohibitive clinical trials. A number of membrane models have emerged to measure permeabilities experimentally and have become prevalent in the pharmaceutical industry. Although such models have proven both effective and useful, accurate theoretical prediction of permeabilities remains a Holy Grail in computer-aided rational drug design. Ideally, in an integrated computational platform, drug candidates that have been ranked according to their binding affinity toward a given target should be subsequently triaged as a function of their bioavailability. A number of methods have been put forth to predict permeabilities at a theoretical level, relying primarily upon empirical rules and structure−activity relationships, or requiring experimental measurements of partition coefficients in organic solvents, which are crude models of the membrane environment. Not too surprisingly, such methods can yield estimates that depart markedly from experiment, calling into question their credibility for the blind determination of bioavailabilities. The shortcomings of empirical models underline the need of a robust methodology, ideally bereft of approximations and capable of providing flawlessly accurate permeabilities from first principles.

To contrive a theoretical approach germane for the computation of permeabilities, establishing as a preamble the formal framework in which this approach is developed is advisable. Passive permeability can be seen from the perspective of a solubility−diffusion model, wherein the permeant partitions first from the aqueous medium to the membrane environment, diffuses amidst the lipids, and ultimately partitions from the membrane to the water phase, on the other side. In the form derived by Marrink and Berendsen,[1] and similar to that of Diamond and Katz,[2] the position-dependent resistance toward permeation is defined by

$$R(z^*) = \int_{\text{bulk}}^{z^*} \mathrm{d}z \frac{\exp[+\beta w(z)]}{D(z)} \tag{1}$$

and is the inverse of the permeability, i.e., $P(z) = R(z)^{-1}$. In eq 1, $w(z)$ is the potential of mean force that delineates the translocation of the permeant across the lipid bilayer and $D(z)$

Received: October 23, 2013
Published: January 15, 2014

   dx.doi.org/10.1021/ct400925s | J. Chem. Theory Comput. 2014, 10, 554−564

is the position-dependent diffusivity. $\beta = (k_B T)^{-1}$, where k_B is the Boltzmann constant and T is the temperature. The expression of the position-dependent resistance, $R(z)$, emphasizes the necessity to have a methodology not only capable of describing the free-energy landscape that underlies the permeation event but also supplies kinetic information about the latter.

The problem of computing passive permeabilities, therefore, reduces to obtaining the functions $w(z)$ and $D(z)$ with a sufficient accuracy. Molecular dynamics is currently the only technique amenable for precise determination of both $w(z)$ and $D(z)$ with high spatial resolution; a number of methodological issues, however, still remain to be addressed. Due to the large differences in hydrophilicity between water and the interior of the membrane, most permeants experience a high free-energy barrier when either entering (relatively hydrophilic molecules) or leaving (relatively hydrophobic molecules) the hydrophobic core of the lipid bilayer. From the standpoint of statistical-mechanics simulations, membrane permeation is usually a rare event, rationalizing why importance sampling techniques are generally required to obtain $w(z)$ with an appreciable accuracy.[3] Previous molecular-dynamics studies of bilayer permeability involve the calculation of potentials of mean force using, for instance, stratified umbrella sampling,[4] stratified umbrella sampling with Hamiltonian exchange,[5] metadynamics on multiple collective variables with bias exchange,[6] determination of the mean force with z being constrained,[1,7] and adaptive biasing force.[8]

Because descriptions of permeant motions by means of $D(z)$ constitute only approximate models, computation of diffusivities requires additional care. Diffusivity estimates may depend on the calculation method,[9−11] the time scale considered,[11,12] the thermostat used in the simulations,[12,13] and the system size.[14] Moreover, it has been suggested that for very narrow channels, diffusive dynamics may not even approximate the motion.[15] To make quantitative comparisons with experiment, such methodological ambiguities must be disentangled.

Certain methods utilized for calculating $w(z)$ have appeared more convenient for the determination of $D(z)$. Because umbrella sampling is by and large performed with a harmonic biasing potential, results for valid Generalized Langevin equation in a harmonic potential[9,16,17] have commonly been used to approximate position-dependent diffusivities[10,18−20] including for passive bilayer permeation.[4] Another approach for determining $D(z)$ is also derived from the generalized Langevin equation,[9] and, in the case of bilayer permeation, involves the autocorrelation function of the stochastic force with z constrained.[1,8] It is possible that other approaches for constructing diffusive models, for example, those described in refs.,[21−23] could be fruitfully adapted to calculate bilayer permeabilities.

Finally, a flexible class of approaches to calculating position-dependent diffusivities assumes a particular diffusive model (ordinarily overdamped Langevin dynamics) and applies a maximum-likelihood[6,24,25] or Bayesian scheme[12,17,26] to determine the model parameters that are most consistent with the observed,[26] or simulated, trajectories. One unique feature of the method used in this work, that of Comer et al.,[12] is it can be used to calculate the time-dependent diffusivity directly from simulations where a time-dependent bias was applied, unlike other methods,[6] where additional unbiased simulations are required.

Although molecular-dynamics investigations have demonstrated the potential of purely theoretical calculations of passive permeabilities,[4,6,8] direct quantitative correspondence between experiments and simulations remains elusive. The possible discrepancies are partially due to the fact that some experimental assays are often not performed with pure lipid bilayers, but with mixtures of organic solvents and egg lecithin[27−29] or with Caco-2 cells,[30,31] which are difficult to model readily in computer simulations. In such cases, quantitative agreement is not expected; yet, even a qualitative comparison has been less than optimal.[4] Even when quantitative agreement should in principle be achieved, differences larger than an order of magnitude have been reported.[1,6] As argued by Ghemei and Laio,[6] some of these differences may be due to misinterpretations of the experimental data; failures in the simulation techniques remain, however, likely culprits.

In this work, we are attempting to address the following questions. Are molecular-dynamics simulations of lipid bilayer permeabilities capable of quantitative agreement with experiment? How can simulation parameters, such as the description of the permeant, the truncation of short-range intermolecular interactions, and the thermostatting algorithm, and possible system-size dependence affect the results? What is the role of the time scale over which the displacements are observed?

The extent to which molecular-dynamics simulations mirror the reality is governed by the accuracy of the set of potential-energy functions describing atomic interactions, otherwise known as the force field. Accurate calculation of membrane permeabilities evidently requires accurate representations of the lipids, water, the permeant and their mutual interactions. Transferable force fields for novel drug-like compounds have made strides in recent years;[32,33] however, significant uncertainties about their accuracy for any individual molecule persist. Despite the importance of such force fields, we will not address them here, choosing to focus on water, a well characterized molecule, for which much experimental validation is available. As will be seen hereafter, overlooked subtleties still remain even for such a prototypical systems.

Academic biomolecular force fields[34−37] have traditionally been optimized to reproduce static properties, such as mean structures, root-mean-square fluctuations, and enthalpies or free energies of solvation, which are determined experimentally or by quantum-mechanical calculations. Kinetic properties are much less often considered in force-field optimization. For this reason, accurate calculations of dynamic properties like permeabilities are complicated by the fact that the kinetic picture rendered by biomolecular force fields is, in some cases, known to deviate significantly from experiment and, in many others, simply untested.

Notably, the TIP3P water model, a slight variant of which has been used in the calibration of the popular CHARMM[34] and AMBER[35] force fields, nominally possesses a self-diffusion coefficient almost three times as large as the experimentally determined value.[14] The discrepant nature of TIP3P diffusivity has been handled by scaling calculated quantities such as permeabilities by D_{exp}/D_{TIP3P}, the ratio of the self-diffusion coefficient of bulk water in experiment to that in simulations using the TIP3P model.[38] However, it is far from clear that scaling based on the bulk values yields correct results in distinct environments, e.g., water confined to narrow channels, or an isolated water molecule within a lipid bilayer.

In addition to TIP3P, we consider an alternative water model, namely TIP4P-Ew,[39] the self-diffusion coefficient of which is much closer to that measured in experiment, and can presumably be used without the need of any correction. The danger in associating an alternate water model to the CHARMM36 lipid force field, which was originally parametrized with TIP3P, is an

imbalance in crucial intermolecular interactions, possibly resulting in incorrect estimates of carefully calibrated quantities like free energies of solvation.[34] Notwithstanding this caveat, a number of studies[40,41] give us confidence that an alternative to TIP3P is at least worth consideration, as they show that substitution of water models does not necessarily degrade the performance of biomolecular force fields and can in some cases improve the agreement with experiment. Water makes a good permeant candidate, because its high concentration in realistic molecular assemblies, i.e., about 55 mol/L, yields a high rate of permeation events, thus allowing our methods to be validated by direct calculation of permeability. Furthermore, popular water models have been amply probed and their shortcomings are well documented.

We have chosen the CHARMM36 all-atom force field[42] to model the lipids because it yields structural and energetic properties of bilayers in good agreement with experiment. Moreover, one kinetic parameter, namely the relaxation rates of tail carbon atoms in 1,2-dipalmitoyl-*sn*-phosphatidylcholine (DPPC) bilayers, was considered in its development. However, for the lipid considered here, i.e., 1-palmitoyl-2-oleoyl-*sn*-phosphatidylcholine (POPC), an important structural parameter, the area per lipid, shows only modest agreement with experiment. Symptomatic treatments of this discrepancy include fixing the membrane area, resulting effectively in an applied surface tension.[43] Here, we consider another symptomatic treatment of this apparent problem, reducing the distance at which the van der Waals force is brought to zero, often referred to as the cutoff, for the simple reason that it increases the performance of the simulations by a factor of two or more, while also giving areas per POPC molecule nearer to experiment. Performance cannot be ignored for simulations like those in this work, where statistical error and quasi nonergodicity constitute limiting factors on accuracy. We present here the effects of reducing the short-range-interaction cutoff on the calculated $w(z)$ and $D(z)$, and, ultimately, on the permeability.

An additional factor affecting dynamics in molecular-dynamics simulations is the thermostatting algorithm used to maintain the temperature constant.[13] Depending on the strength of the coupling parameter, the popular Langevin thermostat can have a large effect on diffusivities.[12,13] However, usually considered detrimental, this property could be exploited to obtain the correct bulk diffusivity for TIP3P, albeit with the risk of unphysical side effects on the permeant dynamics within the bilayer. Furthermore, use of a Langevin thermostat is questionable for transport phenomena, because it presupposes a preferred rest frame and, thus, does not conserve momentum. Here, we, therefore, compare permeant kinetics under Langevin dynamics with that of molecular dynamics equipped with a Lowe–Andersen thermostat,[44] a momentum conserving thermostat.

A further complication in the calculation of the permeability from first principles arises from the small size of typical computer models. Notably, the model bilayer patch must be large enough to accommodate distortions of the bilayer structure, which may occur when the permeant penetrates the bilayer at different heights. Finite-size artifacts due to long-range hydrodynamic interactions have also been shown to bias diffusivity calculations.[14] Thus, as a final test of the effects of simulation protocols on computed permeabilities, we compare the results obtained from the solvated bilayer of minimal size used in a majority of the simulations in this work to those of a system featuring more than twice the number of lipids and almost five times as many water molecules.

2. THEORETICAL UNDERPINNINGS

We have developed a methodology,[12] based on the groundwork laid by Hummer[17] and Türkcan, Alexandrou, and Masson,[26] which reconciles the thermodynamic and dynamic views of the permeation process, obviating the need to run independent simulations to access, on the one hand, $w(z)$, and on the other hand, $D(z)$. In a nutshell, we construct an inverse solution to the Smoluchowski equation, wherein, given the trajectory and the biasing force, we infer the free-energy change and the position-dependent diffusion coefficient using Bayes' theorem.

The adaptive biasing force[45,46] simulations provide trajectories of the transition coordinate, $Z(t)$, here, the component along the bilayer normal of the vector between the center of mass of the bilayer and the center of mass of the tagged permeant. As a matter of notation, we make a distinction between $Z(t)$, a simulation-derived trajectory along the transition coordinate, and the transition coordinate as an independent variable, z. The applied biasing force, $f_{\text{bias}}(t)$, is also recorded throughout the simulation. Assuming a particular diffusive model, in this case, Brownian motion in the overdamped Langevin regime, we can calculate the probability of the trajectory given trial forms of the model parameters[12]

$$P[Z(t)|w_k(z), D_k(z)] = \prod_i \frac{1}{\sqrt{4\pi D_k(Z_i)\Delta t}} \exp\left(-\frac{\{Z_{i+1} - Z_i - \beta D_k(Z_i)[f_{\text{bias}}(t) - \nabla w_k(Z_i)]\Delta t - \nabla D_k(Z_i)\Delta t\}^2}{4D_k(Z_i)\Delta t} \right) \tag{2}$$

where $w_k(z)$ and $D_k(z)$ are the trial position-dependent free energy and diffusivity. The trajectory is discretized by $Z_i = Z(i\Delta t)$. Bayes' theorem[47,48] allows this probability to be "reversed". The probability of the model parameters given the trajectory, also known as the posterior probability, is obtained from the probability of the trajectory given the model parameters by

$$P[w_k(z), D_k(z)|Z(t)] \propto P[Z(t)|w_k(z), D_k(z)]p_{\text{prior}}[w_k(z), D_k(z)] \tag{3}$$

where p_{prior} is the prior probability of the model parameters. The role of $D(z)$ as a scaling factor calls for a scale-invariant prior distribution,[49] i.e., $p_{\text{scale}} = \prod_j 1/D(z_j)$, where z_j represents equally spaced points along the transition coordinate. We furthermore assume that $w(z)$ and $D(z)$ are locally smooth[17]

$$p_{\text{smooth}} = \sum_{j=2}^{n} \exp\left(-\frac{[D(z_j) - D(z_{j-1})]^2}{2\varepsilon_D^2} - \frac{[w(z_j) - w(z_{j-1})]^2}{2\varepsilon_w^2} \right) \tag{4}$$

The problem then becomes one of determining the model parameters, $w(z)$ and $D(z)$, which maximize $P[w(z), D(z) \mid Z(t)]$. For this purpose, we introduce small random changes to

dx.doi.org/10.1021/ct400925s | J. Chem. Theory Comput. 2014, 10, 554–564

the model parameters, i.e., $w_{k+1}(z) = w_k(z) + \eta_k(z)$ or $D_{k+1}(z) = D_k(z) + \eta'_k(z)$, using the Metropolis–Hastings algorithm[50] to sample the parameters that contribute most to the posterior distribution.

The strength of this formulation lies in the possibility to access diffusivities from a free-energy calculation that incorporates time-dependent biases acting on collective variables. The proposed method ensures consistency of both thermodynamic and kinetic quantities by virtue of the Bayesian-inference scheme embodied in eq 3. Moreover, the method does not merely supply a number, namely the permeability, but instead illuminates the full permeation event, notably by revealing the change in diffusivity across the entire reaction path.

Equation 1 suggests that because $w(z)$ is exponentiated, the numerator is expected to vary typically over several orders of magnitude, whereas the denominator only covers a smaller range of values; thus, the precision of the free energy has a greater influence on the error of the calculated permeability than that of the diffusivity. Yet, as will be seen in the present work, having precise measurements of the position-dependent diffusivity, $D(z)$, is of paramount importance to infer reliable estimates of the permeability.

3. METHODOLOGICAL DETAILS

We have performed several sets of simulations, including adaptive biasing force[45,46] calculations to enhance sampling and access free-energy changes from average forces. Below, we describe the details of these simulations and the application of the adaptive biasing force algorithm After the simulations were completed, the trajectory of the permeant molecule was extracted and subjected to the Bayesian inference method outlined in the above theoretical underpinnings. The practical details of this method are described below.

3.1. Molecular Dynamics Simulations. For the majority of the simulations, use was made of a minimal model of a hydrated bilayer comprising 40 POPC molecules and 1878 water molecules. The periodic cell was a hexagonal prism, having an x,y cross section formed by regular hexagons. The z axis was conventionally defined as the normal to the bilayer. The initial atomic positions were generated using the MembraneBuilder plugin of VMD.[51] To investigate the possibility of size dependence, a larger square-prismatic system was also constructed, consisting of 100 POPC units hydrated by 9294 water molecules.

The molecular dynamics simulations were performed using NAMD 2.9,[52] with the particle mesh Ewald algorithm[53] for long-range electrostatic interactions (mesh spacing <0.12 nm) and the r-RESPA multiple time-step integrator[54] with time steps of 2 and 4 fs for short- and long-range interactions. The SETTLE[55] algorithm maintained the rigid geometry of the water molecules, while RATTLE[56] constrained the length of covalent bonds featuring hydrogen atoms. The temperature was kept constant at 308 K, either by a Langevin thermostat with a damping constant of 1 ps^{-1}, or, wherever indicated, by the Lowe–Andersen thermostat, using the default parameters of NAMD 2.9 (a cutoff of 0.27 nm and a rate of 50 ps^{-1}). The pressure was kept constant at 101.325 kPa by means of the Langevin piston method.[57]

Water was represented by the TIP3P water model standard to the CHARMM force field, or, wherever indicated, by the TIP4P-Ew[39] water model. Lipids were described in all-atom detail using the CHARMM36 force field.[42] For consistency with the parametrization of the CHARMM36 force field, a switching function was applied to van der Waals forces. Three different schemes were compared for the cutoff of the van der Waals forces, namely 0.7–0.8, 0.8–0.9, and 10–12 nm, which represents, in each case, the range over which the force is smoothly brought to zero. The drift of the center of mass induced by small errors in the particle mesh Ewald algorithm was removed to conserve momentum in simulations expected to do so, notably those involving the Lowe–Andersen thermostat. Analyses of the simulation were performed in VMD,[51] probing the area per lipid, hydration of the tagged water molecule, and local distortion of the lipid bilayer.

3.2. Free-Energy Calculations. Calculations of potentials of mean force were performed along a single transition coordinate, i.e., the component normal to the bilayer of the vector connecting the center of mass of the nitrogen and phosphorus atoms of all lipids to the center of mass of the tagged water molecule. For efficiency, the calculation was divided into 1.2 nm overlapping windows on the domain $-3.6 < z < 3.6$ nm. The domain was $-0.8 < z < 4.4$ nm for the larger system. The subsequent calculation of the diffusivity required that permeant displacements beginning too close to the window boundary be discarded. Each window, thus, had 0.4 nm of overlap with its neighbors to ensure accurate calculation of the diffusivity throughout the domain. In each window, molecular-dynamics simulations were carried out including an adaptive biasing force[45,46] on the transition coordinate. Local estimates of the mean force were collected in 0.01 nm bins. The simulations were run until a minimum of 600 000 samples was accrued per bin, which represents 100–250 ns of sampling for each window. The total time for a complete calculation amounted to 1–3 μs. All potentials of mean of force were shifted so that the mean over the interval $-3.6 < z < -3.4$ nm, i.e., the region farthest from the bilayer, was zero. The global error in the free-energy profiles was estimated to be the absolute difference between the mean over $-3.6 < z < -3.4$ nm and the mean over $+3.4 < z < +3.6$ nm, because the free energy is, in principle, symmetric about z.

Each calculation began with only two windows, $z \in [1.6,2.8]$ nm and $z \in [2.4,3.6]$ nm, for which the tagged water molecule was above the water–membrane interface. After at least 2 ns, a snapshot satisfying $z < 2.0$ nm was extracted from the trajectory of the former window. This snapshot was then used as an initial condition for the $z \in [0.8,2.0]$ nm window. Initial conditions were generated for all subsequent windows by an analogous process.

3.3. Bayesian Construction of the Diffusive Model. The diffusivity was calculated as a function of the transition coordinate, using the Bayesian scheme outlined in the above theoretical underpinnings, with additional details provided in Comer et al.[12] For each simulation, the trajectory of the tagged permeant molecule, $Z(t)$, and the biasing force, $f_{\text{bias}}(t)$ were extracted at time intervals $\Delta t = 2$ ps. The potential of mean force, $w(z)$, and the diffusivity, $D(z)$, were interpolated from piecewise cubic and piecewise linear polynomials, respectively,[58] defined over $-3.4 < z < 3.4$ nm with a grid spacing of 0.02 nm. The smoothness parameters in eq 4 were set to $\varepsilon_D = 0.04$ nm^2/ns and $\varepsilon_w = 1$ kcal/mol. No additional priors, for instance, restraining $w(z)$ to the result derived from the adaptive biasing force, were applied. For each calculation, 30×10^6 Monte Carlo steps, i.e., random displacements of $w(z)$ or $D(z)$, were attempted, with these displacements taken from a Student's t-distribution with $\nu = 1$ and scaled by $\delta w = 0.02$ kcal/mol and $\delta D = 0.05$ nm^2/ns. The acceptance rates averaged to about 30%. The statistical errors in the diffusivity values were estimated by partitioning the trajectory into two subsets and repeating the Bayesian analysis for each

subset. The plotted symmetric error bars are just large enough to delimit both $D(z)$ functions obtained from the two subsets.

4. RESULTS AND DISCUSSION

In this section, we present the results of the Bayesian scheme outlined in the theoretical underpinnings for different systems. The calculations were performed as a way to understand the influence of different simulation protocols on the permeability and validate the results of the Bayesian method. Table 1 summarizes the parameters defined for each simulation as well as the calculated permeability values.

Table 1. Summary of the Molecular Dynamics Simulations Performed in This Work[a]

calc	# of atoms	water model	cutoff [nm]	thermostat	perm. [10^{-4} cm/s]
A	10994	TIP3P	1.0−1.2	Lang.	64.7 ± 0.9
B	10994	TIP3P	0.8−0.9	Lang.	67.3 ± 0.7
C	10994	TIP3P	0.7−0.8	Lang.	141.2 ± 1.7
D	10994	TIP3P	0.8−0.9	LA	76.4 ± 0.8
E	12872	TIP4P-Ew	0.8−0.9	LA	33.4 ± 0.2
F	41282	TIP3P	0.8−0.9	LA	82.0 ± 0.8
expt[59]					136

[a]"Cutoff" refers to the distances over which the van der Waals force was smoothly brought to zero. "Lang." and "LA" denote the Langevin and Lowe−Andersen thermostat, respectively.

4.1. van der Waals Cutoff. The van der Waals cutoff has an appreciable affect on the structural properties of lipid bilayers in the CHARMM36 force field and should be considered as an integral part of the force field.[42] According to Figure 1, as well as

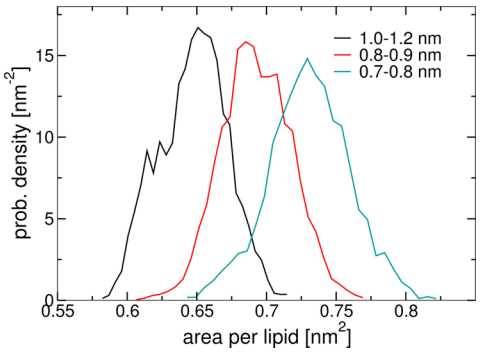

Figure 1. Distributions of area per lipid in unbiased molecular dynamics simulations with different van der Waals cutoffs. The black, red, and cyan lines correspond to the calc A, B, and C, respectively, in Table 1.

the reference article for the force field,[42] CHARMM36 supplemented by standard cutoff parameters, i.e., 1.0−1.2 nm, yields an average area per lipid of about 0.65 nm^2, which is appreciably lower than the experimental value of 0.683 ± 0.015 nm^2 at 308 K. On the other hand, a 0.8−0.9 nm cutoff gives a mean area per lipid significantly closer to experiment, namely 0.69 ± 0.04 nm^2. Of course, better agreement for a single structural parameter does not imply that the 0.8−0.9 nm cutoff is superior in all respects, and a comprehensive validation of other bilayer properties would be prudent as a preamble to its continued use. However, the fact that this cutoff resulted in a 2-fold increase in the performance over the standard cutoff under the conditions of our simulations with NAMD may provide an additional argument in favor of its use. The admittedly radical 0.7−0.8 nm cutoff gives an area per lipid that is considerably too large, i.e., 0.73 ± 0.03 nm^2, furnishing an argument against its use.

Figure 2 shows the potential of mean force (A), the diffusivity (B), and the resistance to permeation per unit length (C), as determined by the adaptive biasing force algorithm, the Bayesian inference scheme and $\exp(+\beta w(z))\,/D(z)$, respectively. For the latter, we antisymmetrized $\nabla w(z)$ and symmetrized $D(z)$ by computing the weighted averages

$$\nabla w_{\mathrm{sym}}(z_j) = [N(z_j)\nabla w(z_j) - N(-z_j)\nabla w(-z_j)] \,/[N(z_j) + N(-z_j)]$$

$$D_{\mathrm{sym}}(z_j) = [N(z_j)D(z_j) + N(-z_j)D(-z_j)] \,/[N(z_j) + N(-z_j)]$$

where $N(z_j)$ is the number of samples in bin j. The permeabilities shown in Table 1 were calculated by integrating over the symmetrized permeation resistance per unit length, in accordance with eq 1.

As can be seen in Figure 2A, the height of the free-energy barrier at the center of the bilayer is correlated with the lipid density, i.e., the systems with smaller areas per lipid show higher energetic barriers. The difference between neighboring cutoffs is not large, typically about 0.2 kcal/mol, which is only moderately larger than the expected statistical error. Note that potentials of mean force are shifted to zero on the left side of Figure 2A; in other words, the free energy is conventionally set to zero when the tagged water molecule lies in the bulk, far from the aqueous interface with the membrane. Deviations from zero on the far right of the plot, where the water molecule also lies in the bulk aqueous medium, away from the membrane, are indicative of the reliability of the potential of mean force. The potential of mean force is calculated by numerical integration of mean forces over the transition coordinate; therefore, free-energy differences, $\Delta G_{a\to b} = w(z_b) - w(z_a) = -\int_{z_a}^{z_b} \mathrm{d}z\, f_{\mathrm{sys}}(z)$, have associated statistical errors that depend on the interval over which the integration is performed.[60] Thus, ΔG values for nearby points have a higher precision than those at points with large separations, and the statistical error for ΔG across the whole domain constitutes an estimate of the upper bound of the statistical error for any two points within the domain.

The position-dependent diffusivity shown in Figure 2B does not differ dramatically between the calculations using different cutoffs, although the diffusivity appears to be somewhat lower in the tail region of the membrane for the 1.0−1.2 nm cutoff, which is likely to stem from the higher lipid density for this systems (see Figure 1). The diffusivity of water is particularly low in the headgroup region of the membrane, a phenomenon that has been ascribed to transient binding of water molecules with the zwitterionic lipid head groups.[1] The diffusivity peaks about half a nanometer from the membrane center, which is almost certainly because the free volume accessible to water molecules in this region is considerably higher than in the rest of the bilayer.[1]

The resistance to permeation per unit length, calculated by $\exp(+\beta w(z))/D(z)$, is shown in Figure 2C. Due to the exponential dependence on $\beta w(z)$, the most significant contributions come primarily from the tail region, $-1 < z < +1$ nm, where the free energy is significantly larger than $k_{\mathrm{B}}T$ (0.61 kcal/mol at 308 K). It is worth noting that although the overwhelming importance of the contributions in this region is likely to hold for other hydrophilic permeants, markedly different

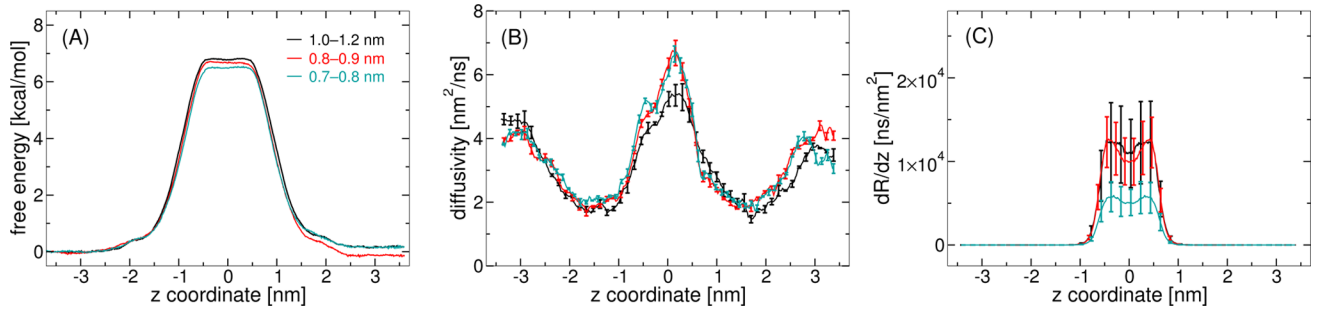

Figure 2. Permeation of water through a POPC bilayer showing dependence on the cutoff distance of the van der Waals force. (A) Free energy as a function of position with respect to the central plane of the bilayer. (B) Diffusivity as a function of position with respect to the central plane of the bilayer. (C) Permeation resistance per unit length as a function of position with respect to the central plane of the bilayer. The black, red, and cyan lines correspond to the calc A, B, and C in Table 1.

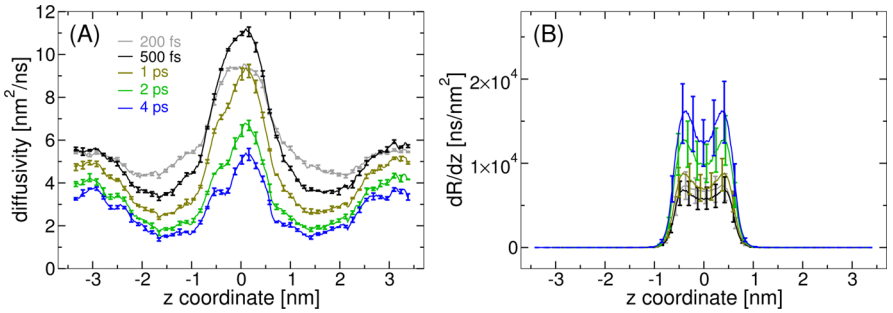

Figure 3. Position-dependent diffusivity and permeation resistance per unit length for Bayesian analyses with different time intervals between displacements. All curves are derived from analysis of calc B (cf. Table 1).

behavior is to be expected for hydrophobic permeants. The predicted resistance to permeation is the area under the curves in Figure 2C. In the tail region of the bilayer, the system with 0.7−0.8 nm cutoff has both a smaller free-energy barrier and a higher diffusivity. It is, therefore, endowed with a significantly lower resistance to permeation. On the other hand, the 1.0−1.2 nm and 0.8−0.9 nm cutoffs show comparable resistances per unit length due to the fact that the increased free-energy barrier for the 1.0−1.2 nm cutoff is partially compensated by the lower diffusivity near the center of the membrane.

For the permeabilities, we obtain 141 ± 2, 67.3 ± 0.7, and 64.7 ± 0.9, in units of 10^{-4}cm/s, for the 0.7−0.8, 0.8−0.9, 1.0−1.2 nm cutoffs, respectively. The reported experimental value at 308 K, obtained from nuclear magnetic relaxation dispersion, is equal to 136×10^{-4} cm/s.[59] Although the 0.7−0.8 nm cutoff appears to give a value of the permeability closer to experiment, the agreement may be incidental as discussed in Conclusions. Owing to the similarity of the permeabilities with the 0.8−0.9 and 1.0−1.2 nm cutoffs, as well as the better performance of the simulations and the agreement with experiment for the area per lipid with an 0.8−0.9 cutoff, we made use of the 0.8−0.9 nm cutoff to probe the influence of all other simulation parameters on the calculated permeability, as is discussed hereafter.

Our results are in qualitative agreement with those presented by Marrink and Berendsen.[1] However, likely due to the higher temperature (350 K) and use of a different lipid and force field, which included the united-atom GROMOS[61] force field for 1,2-dipalmitoyl-*sn*-glycero-3-phosphocholine (DPPC) lipids[62] and the SPC water model, there are quantitative differences. The free-energy barrier at the center of the bilayer appears diminished by about $2k_BT$. Although we observe a somewhat larger diffusivity in the low-density tail region than in the bulk, Marrink and Berendsen recorded a diffusivity several times larger, which we attribute to the lack of explicit hydrogen atoms in the GROMOS lipid model.[62] Although the ability of united-atom force fields to reproduce static properties compares favorably to all-atom force fields,[63,64] whether all-atom models exhibit more realistic kinetic properties compared to united-atom models remains an open question that ought to be explored further.

4.2. Diffusion Time Scale. Most real systems possess multiple kinetic regimes spanning different time scales. At sufficiently short times, molecular motion is ballistic, whereas for very long times, inertia typically becomes negligible and the motion becomes uncorrelated and describable by classical Brownian dynamics. Even beyond the time scale of ballistic motion, complex interactions within the systems can lead to multiple diffusive regimes, which is well-known for diffusion of lipids or other molecules within lipid bilayers[6,65−67] and other biological systems.[11,68−70] $D(z)$ is, thus, not necessarily well-defined, as manifested in the fact that naively calculated diffusivities depend on the time scale over which displacements are observed.[17,12] Figure 3 shows the diffusivity and permeation resistance per unit length predicted with different Δt values for calc B. For permeation, we are interested in the long-time limit of the diffusivity; going to long times, however, violates the assumptions of discretization in eq 2. As this paper was revised, we implemented a similar method to that described here, yet in which the discretization time scale was independent of the time over which the displacements were observed. Using a small, fixed Δt (500 fs) while setting the observation time scale to 1, 2, and 4 ps yielded curves essentially identical to those shown in Figure 3. Therefore, the time scale dependence cannot be attributed to discretization error, but must be due to the existence of different kinetic regimes. The diffusivity in the center of the bilayer appears particularly sensitive to the time scale, a situation that complicates the calculation of the permeability, because this

dx.doi.org/10.1021/ct400925s | J. Chem. Theory Comput. 2014, 10, 554−564

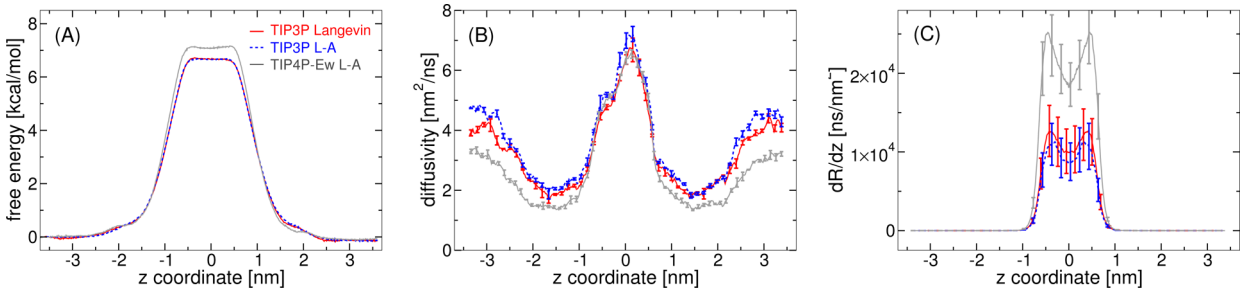

Figure 4. Permeation of water through a POPC bilayer showing differences due to different thermostats and water models. (A) Free energy as a function of position with respect to the central plane of the bilayer. (B) Diffusivity as a function of position with respect to the central plane of the bilayer. (C) Permeation resistance per unit length as a function of position with respect to the central plane of the bilayer. The red, blue, and gray curves correspond to calc B, D, and E (cf. Table 1), respectively.

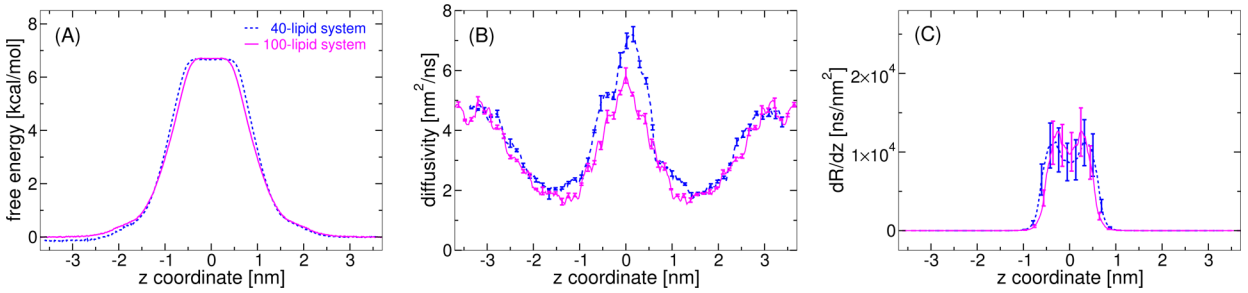

Figure 5. Permeation of water through a POPC bilayer showing differences due the size of the simulated system. (A) Free energy as a function of position with respect to the central plane of the bilayer. (B) Diffusivity as a function of position with respect to the central plane of the bilayer. (C) Permeation resistance per unit length as a function of position with respect to the central plane of the bilayer. The blue and magenta curves correspond to calcs D and F, respectively (cf. Table 1). Due to the much greater computational expense of the 100-lipid system, the calculation for the 100-lipid system was performed only on the domain $-4.4 < z < +0.4$ nm and symmetrized to obtain the plots shown here.

region contributes the most to the latter. For the remainder of this work, we have chosen $\Delta t = 2$ ps, a choice validated hereafter by observing spontaneous permeation in an equilibrium, i.e., unbiased simulation.

4.3. Validation by Observation of Spontaneous Permeation. We performed a 1.7 μs unbiased equilibrium simulation with a 0.7−0.8 nm cutoff on van der Waals interactions to calculate the permeability directly. Over the simulation, we observed 106 instances where water molecules completely translocated across the bilayer, corresponding to a permeabililty of $(134 \pm 13) \times 10^{-4}$ cm/s. This value compares well with the value derived from the application of eq 1 to the data in Figure 2C, namely $(141 \pm 2) \times 10^{-4}$ cm/s. The comparison between spontaneous permeation and importance sampling calculations based on adaptive biasing force and the Bayesian inference scheme is made feasible by the use of water as a permeant. At realistic concentrations, other permeants would require simulations at least 2 orders of magnitude longer (or larger) to obtain permeabilities with the same relative error.

Two models have been proposed to describe passive permeation, the solubility−diffusion model, implicit in our use of eq 1, and the transient defect model.[59] Each spontaneous permeation event observed in our simulation involved only an isolated water molecule, supporting the solubility−diffusion model for water permeation and validating the use of $w(z)$ and $D(z)$, which were determined for isolated water molecules. The alternative transient defect model suggests the formation of pore-like structures, which were not observed on the microsecond time scale of our simulations.

4.4. Choice of the Thermostat. A Langevin thermostat with a damping constant of 1 ps^{-1} tends to reduce the diffusivity with respect to simulations devoid of a thermostat. In the case of bulk TIP3P water, the self-diffusion coefficient is about 15% lower. On the other hand, the Lowe−Andersen thermostat, at least with the parameters employed here (see Methodological Details), seems to have no appreciable effect on the bulk self-diffusion coefficient with respect to simulations with no thermostat. Figure 4 illustrates the differences in kinetics that arise from these two thermostats. In principle, the choice of a thermostat should have no effect on the energetic properties of the system. Correspondingly, Figure 4A shows no appreciable difference in the potential of mean force between the calculation with the Langevin thermostat and that with the Lowe−Andersen thermostat. The choice of thermostat does, however, have a small, but appreciable, effect on the diffusivity, as shown in Figure 4B. It appears that the Langevin thermostat depresses the diffusivity within the bilayer by about 10%. With the Lowe−Andersen thermostat, we obtain a permeability of $(76.4 \pm 0.8) \times 10^{-4}$ cm/s, significantly higher and slightly closer to the experimental value than that with the Langevin thermostat, $(67.3 \pm 0.7) \times 10^{-4}$ cm/s.

4.5. Role of the Water Model. The TIP3P water model, however popular, suffers from many shortcomings, including a bulk self-diffusion coefficient almost 2 orders of magnitude larger than the value determined experimentally.[14] One would, therefore, hope that a water model, such as TIP4P-Ew[39] endowed with a more accurate bulk self-diffusion coefficient might yield more accurate predictions of lipid-bilayer permeabilities. However, because the permeability depends almost exclusively on the diffusivity within 1 nm from the center of the membrane, the self-diffusion of bulk water has little importance for the calculation of the permeability. Moreover, it is not certain

dx.doi.org/10.1021/ct400925s | J. Chem. Theory Comput. 2014, 10, 554−564

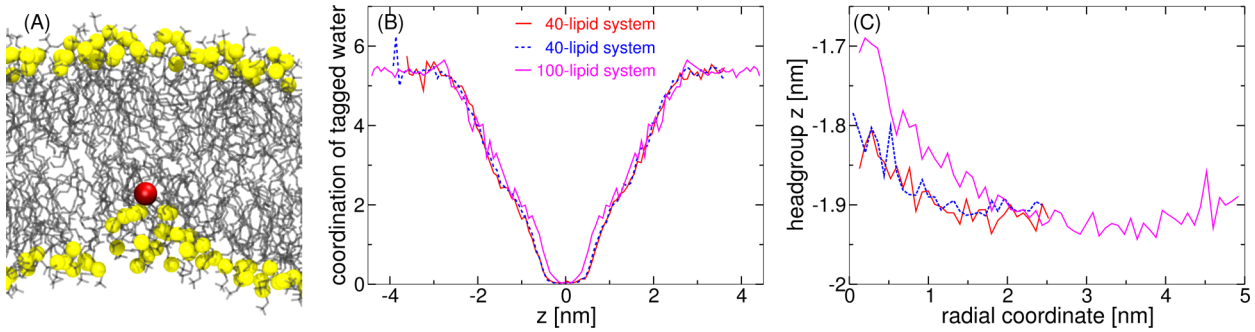

Figure 6. Bilayer distortion due to the penetration of the permeant for simulated systems of two different sizes. (A) Simulation snapshot showing typical bilayer distortion when the permeating water molecule is near the center of the membrane in the 100-lipid system. Lipid headgroup phosphorus atoms are highlighted as yellow spheres, whereas the remaining heavy atoms of the lipids are shown as gray tubes. The tagged water molecule is shown as a red sphere. For clarity, other water molecules are not represented. (B) Number of water molecules coordinating the permeating water molecule. (C) Position of headgroup phosphorus atoms with respect to the center of mass of the bilayer as a function of lateral distance from the tagged water molecule. The tagged water molecule lies in the range $-0.5 < z < 0.0$ nm. The curves are essentially the average cross sections of bilayer distortions like that seen in panel A, showing clear depressions near the tagged water molecule. The red, blue, and magenta lines correspond to calc B, D, and F, respectively (cf. Table 1).

that the improved kinetic properties of bulk TIP4P-Ew with respect to bulk TIP3P necessarily implies better kinetics and energetics for an isolated water molecule within the tail region of the bilayer, especially considering that the lipid force field was calibrated with TIP3P. Keeping all this in mind, we considered the permeability of the bilayer for the TIP4P-Ew water model. First, we note a slight difference in the free-energy barrier for crossing the membrane, i.e., 7.1 kcal/mol, as opposed to 6.7 kcal/mol in the case of TIP3P. This difference is for many purposes small; however, by itself, it leads to a change in the permeability by a factor of 2. Consistent with Horn et al.,[39] we observe a significantly lower bulk diffusivity for TIP4P-Ew than in any of the TIP3P simulations. Due to the larger free-energy barrier, a much higher resistance to permeation was computed with TIP4P-Ew, yielding a permeability, $(33.4 \pm 0.2) \times 10^{-4}$ cm/s, several times smaller than the experimental value.

4.6. System Size and Distortion of the Bilayer. Up until this point, all calculations considered here were performed using a 40-lipid bilayer model. To determine the possible influence of the system size on the permeability, a similar analysis was carried out on a 100-lipid bilayer model, which, in addition to the increased area of the bilayer, was also larger along the bilayer normal (12 versus 8 nm). The simulation parameters were the same as those of calc D (see Table 1). In Figure 5, we compare the free energy, the diffusivity, and the resistance to permeation per unit length of the latter and the calculation that used the larger system, calc F. The free-energy profiles shown in Figure 5A appear slightly different. Although the height of the barrier is the same within the precision of the calculation, the barrier is somewhat narrower for the larger system. Furthermore, the diffusivity near the center of the bilayer is perceptibly lower, as shown in Figure 5B. The effects on the free-energy profile and diffusivity partially cancel one another, although the narrower barrier in the case of the larger system has the greatest effect, yielding a permeability of $82.0 \pm 0.8 \times 10^{-4}$ cm/s, somewhat higher than for the smaller system, $76.4 \pm 0.8 \times 10^{-4}$ cm/s.

The difference in the permeability between the small and large systems is moderate compared to that between the calculations using different water models, for instance; however, as discussed below, the origin of this difference gives insight into the microscopic details of permeation and may prove critical for larger permeants. Previous work[14] has identifed finite-size artifacts due to hydrodynamic interactions between periodic images; however, this artifact does not appear to predominate here. Figure 5B reveals that the diffusivity far from the membrane ($|z| > 3$ nm) does not differ substantially between the 40- and 100-lipid systems. Morever, the difference in the free-energy profiles (Figure 5A) demonstrates that the effect cannot be purely hydrodynamic.

Figure 6 reveals how structure of the bilayer is perturbed by the presence of the permeating water molecule. It has been shown previously that polar and amphiphilic permeants are often accompanied by a column of water that extends into the bilayer during the permeation process.[71] For a permeating water molecule, we observe such a column of water, the existence of which implies a distortion of the bilayer structure during the permeation process, as exemplified in Figure 6A. Figure 6B shows the number of water molecules within 0.35 nm of the permeant as a function of the transition coordinate, i.e., the distance between the center of mass of the permeant and that of the bilayer. The permeating water molecule remains on average partially solvated until reaching the very center of the bilayer, with solvation persisting to a slightly greater penetration depth for the 100-lipid system than for the 40-lipid system.

The structure shown in Figure 6A is not rare. In Figure 6C, we plot the mean z coordinate of the phosphorus atoms of the lower bilayer leaflet as a function of distance from the tagged water molecule projected onto the plane of the bilayer. The distances were collected when the permeant lay in the lower leaflet and near the center of the bilayer, specifically for $-0.5 < z < 0.0$ nm. For the 100-lipid system, the distortion of the bilayer extends laterally from the tagged water molecule to about 3.0 nm, which is slightly larger than the lateral size of the 40-lipid system. The 40-lipid system is unable to undergo distortion to the same extent seen for the 100-lipid system. The observed structural deformation enables the tagged water molecule to get closer to the center of the bilayer without being completely desolvated, which is clear from Figure 6B. We can then rationalize why the bilayer appears effectively thinner for the 100-lipid system than for the 40-lipid system in Figure 5A, and why the diffusivity differs between the two systems. We conclude that the 40-lipid system used extensively in this work is somewhat too small and shows an appreciable finite-size artifact due to the fact that the bilayer is unable to embrace the extent of the distortion witnessed for the 100-lipid bilayer. It ought to be remembered, however, that the effect on the calculated permeability is not large (<10%).

dx.doi.org/10.1021/ct400925s | J. Chem. Theory Comput. 2014, 10, 554−564

5. CONCLUSION

As prediction of bioavailabilities are becoming an important component of computer-aided rational drug discovery, having access to permeabilities from first principles is highly desirable. Efforts to determine permeabilities following a solubility−diffusion model and using statistical mechanics simulations have been hitherto thwarted by difficulties to reliably compute the free-energy landscape that underlies the passage of the drug across model membranes and the associated diffusivity. Having laid the groundwork to reconcile thermodynamics and kinetics in importance-sampling simulations by means of a Bayesian-inference scheme, wherein the parameters of the Smoluchowski equation, namely the potential of mean force and the position-dependent diffusion coefficient, are determined self-consistently, we have further leveraged the approach to calculate permeabilities.

As a cogent illustration, water was chosen as a permeant, allowing a physically meaningful number of translocation events to be witnessed in equilibrium, i.e., unbiased simulations, and, thus, offering a convenient framework to validate our method. Using Δt = 2 ps in the Bayesian-inference scheme is shown to constitute a reasonable choice, giving a ∼0.1 nm spatial resolution, while also yielding results congruent with the direct observation of the permeability. The permeability of water through a POPC bilayer has been computed for different parameters of the simulation, including the truncation of short-range interactions, the force field, the thermostat, and the size of the molecular assembly.

The simulation using a 0.7−0.8 nm van der Waals cutoff and a Langevin thermostat with a damping constant of 1 ps^{-1} yielded the best agreement with the experimental permeability, namely $(141 \pm 2) \times 10^{-4}$ versus 136×10^{-4} cm/s. We do not venture, however, to suggest that these parameters represent the best possible choice, as the Langevin thermostat artificially reduces the diffusivity and a 0.7−0.8 nm van der Waals cutoff leads to a POPC bilayer having too large an area per lipid. The Lowe−Andersen thermostat appears to offer a more realistic picture of the kinetics, whereas the 0.8−0.9 nm cutoff yields a POPC bilayer structure with a density noteworthily closer to experiment. The set of simulation parameters combining the Lowe−Andersen thermostat, a 0.8−0.9 nm van der Waals cutoff, the TIP3P water model, and the 100-lipid membrane might, indeed, constitute a good candidate for the best a priori estimate of the permeability. The latter combination of parameters, however, gives a permeability about 60% of that measured in experiments. Suggesting a theoretically sound choice of simulation parameters that gives close agreement between calculated and experimental permeabilities is admittedly a daunting challenge at this time.

The Bayesian scheme used here to calculate the position-dependent diffusivity appears to be limited by extent to which the discretized Brownian dynamics propagator can describe the permeant kinetics. It is possible to reduce adverse effects of discretization error by modifying the propagator; however, this modification was not found to appreciably affect the results presented here. Development of more robust kinetic models, incorporating, for example, anomalous diffusion,[70] or rotational degrees of freedom[72] may permit the permeation process to be better characterized.

The source of the discrepant experimental and theoretical estimates may in all likelihood be ascribed to imperfections in the force field. The permeability is acutely sensitive to the height of the free-energy barrier to translocation, centered at the middle of the bilayer. An error as large as 0.4 kcal/mol in this height changes the permeability by a factor of two. Furthermore, considering that little attention has been paid hitherto to kinetics in force-field calibration, there is a greater uncertainty in the computed diffusivities than in the free energies. It would not be surprising if a factor-of-two error in the diffusivity (and, hence, in the permeability) were of systematic origin, i.e., rooted in the force field. We expect that, with improvements of the force fields (particularly those yielding improved descriptions of permeants in the lipid bilayer environment), quantitatively accurate prediction of permeabilities of small molecules will be attained.

AUTHOR INFORMATION

Corresponding Author

*C. Chipot. E-mail: chipot@ks.uiuc.edu.

Notes

The authors declare no competing financial interest.

ACKNOWLEDGMENTS

The authors are indebted to the Centre Informatique National de l'Enseignement Supérieur in Montpellier, France, for provision of a generous amount of computer time.

REFERENCES

(1) Marrink, S.; Berendsen, H. Simulation of Water Transport through a Lipid Membrane. *J. Phys. Chem.* **1994**, *98*, 4155−68.

(2) Diamond, J. M.; Katz, Y. Interpretation of Nonelectrolyte Partition Coefficients between Dimyristoyl Lecithin and Water. *J. Membrane Biol.* **1974**, *17*, 121−154.

(3) Chipot, C.; Pohorille, A. *Free Energy Calculations*; Springer: Berlin, Heidelberg, New York, 2007.

(4) Swift, R. V.; Amaro, R. E. Back to the Future: Can Physical Models of Passive Membrane Permeability Help Reduce Drug Candidate Attrition and Move Us Beyond QSPR? *Chem. Biol. Drug Des.* **2013**, *81*, 61−71.

(5) Neale, C.; Madill, C.; Rauscher, S.; Pomès, R. Accelerating Convergence in Molecular Dynamics Simulations of Solutes in Lipid Membranes by Conducting a Random Walk Along the Bilayer Normal. *J. Chem. Theory Comput.* **2013**, *9*, 3686−3703.

(6) Ghaemi, Z.; Minozzi, M.; Carloni, P.; Laio, A. A Novel Approach to the Investigation of Passive Molecular Permeation through Lipid Bilayers from Atomistic Simulations. *J. Phys. Chem. B* **2012**, *116*, 8714−8721.

(7) Bemporad, D.; Essex, J. W.; Luttmann, C. Permeation of Small Molecules through a Lipid Bilayer: a Computer Simulation Study. *J. Phys. Chem. B* **2004**, *108*, 4875−4884.

(8) Wei, C.; Pohorille, A. Permeation of Nucleosides through Lipid Bilayers. *J. Phys. Chem. B* **2011**, *115*, 3681−3688.

(9) Mamonov, A.; Kurnikova, M.; Coalson, R. Diffusion Constant of K + inside Gramicidin A: a Comparative Study of Four Computational Methods. *Biophys. Chem.* **2006**, *124*, 268−278.

(10) Chen, H.; Ilan, B.; Wu, Y.; Zhu, F.; Schulten, K.; Voth, G. A. Charge Delocalization in Proton Channels. I. The Aquaporin Channels and Proton Blockage. *Biophys. J.* **2007**, *92*, 46−60.

(11) Zlenko, D. Computing the Self-diffusion Coefficient for TIP4P Water. *Biophys.* **2012**, *57*, 127−132.

(12) Comer, J. R.; Chipot, C. J.; Gonzalez-Nilo, F. D. Calculating Position-dependent Diffusivity in Biased Molecular Dynamics Simulations. *J. Chem. Theory Comput.* **2013**, *9*, 876−882.

(13) Basconi, J. E.; Shirts, M. R. Effects of Temperature Control Algorithms on Transport Properties and Kinetics in Molecular Dynamics Simulations. *J. Chem. Theory Comput.* **2013**, *9*, 2887−2899.

(14) Yeh, I.-C.; Hummer, G. System-size Dependence of Diffusion Coefficients and Viscosities from Molecular Dynamics Simulations with Periodic Boundary Conditions. *J. Phys. Chem. B* **2004**, *108*, 15873−15879.

(15) Wilson, M. A.; Wei, C.; Bjelkmar, P.; Wallace, B. A.; Pohorille, A. Molecular Dynamics Simulation of the Antiamoebin Ion Channel: Linking Structure and Conductance. *Biophys. J.* **2011**, *100*, 2394−2402.
(16) Woolf, T. B.; Roux, B. Conformational Flexibility of o-phosphorylcholine and o-phosphorylethanolamine: a Molecular Dynamics Study of Solvation Effects. *J. Am. Chem. Soc.* **1994**, *116*, 5916−5926.
(17) Hummer, G. Position-dependent Diffusion Coefficients and Free Energies from Bayesian Analysis of Equilibrium and Replica Molecular Dynamics Simulations. *New J. Phys.* **2005**, *7*, 34.
(18) Luo, Y.; Egwolf, B.; Walters, D.; Roux, B. Ion Selectivity of α-Hemolysin with a β-Cyclodextrin Adapter. I. Single Ion Potential of Mean Force and Diffusion Coefficient. *J. Phys. Chem. B* **2009**, 2035−2042.
(19) Hénin, J.; Tajkhorshid, E.; Schulten, K.; Chipot, C. Diffusion of Glycerol through *Escherichia Coli* Aquaglyceroporin GlpF. *Biophys. J.* **2008**, *94*, 832−839.
(20) Zhu, F.; Hummer, G. Theory and Simulation of Ion Conduction in the Pentameric GLIC Channel. *J. Chem. Theory Comput.* **2012**, *8*, 3759−3768.
(21) Gullingsrud, J. R.; Braun, R.; Schulten, K. Reconstructing Potentials of Mean Force through Time Series Analysis of Steered Molecular Dynamics Simulations. *J. Chem. Phys.* **1999**, *151*, 190−211.
(22) Adib, A. B. Random-walk Approach to the d-dimensional Disordered Lorentz Gas. *Phys. Rev. E: Stat., Nonlinear, Soft Matter Phys.* **2008**, *77*, 021118.
(23) Teo, I.; Schulten, K. A Computational Kinetic Model of Diffusion for Molecular Systems. *J. Chem. Phys.* **2013**, *139*, 121929.
(24) Micheletti, C.; Bussi, G.; Laio, A. Optimal Langevin Modeling of Out-of-equilibrium Molecular Dynamics Simulations. *J. Chem. Phys.* **2008**, *129*, 074105.
(25) Marinelli, F.; Pietrucci, F.; Laio, A.; Piana, S. A Kinetic Model of Trp-cage Folding from Multiple Biased Molecular Dynamics Simulations. *PLoS Comp. Biol.* **2009**, *5*, e1000452.
(26) Türkcan, S.; Alexandrou, A.; Masson, J. A Bayesian Inference Scheme to Extract Diffusivity and Potential Fields from Confined Single-Molecule Trajectories. *Biophys. J.* **2012**, *102*, 2288−2298.
(27) Finkelstein, A. Water and Nonelectrolyte Permeability of Lipid Bilayer Membranes. *J. Gen. Physiol.* **1976**, *68*, 127−135.
(28) Orbach, E.; Finkelstein, A. The Nonelectrolyte Permeability of Planar Lipid Bilayer Membranes. *J. Gen. Physiol.* **1980**, *75*, 427−436.
(29) Xiang, T.-X.; Anderson, B. The Relationship Between Permeant Size and Permeability in Lipid Bilayer Membranes. *J. Membr. Biol.* **1994**, *140*, 111−122.
(30) Adson, A.; Burton, P. S.; Raub, T. J.; Barsuhn, C. L.; Audus, K. L.; Ho, N. F. Passive Diffusion of Weak Organic Electrolytes Across Caco-2 Cell Monolayers: Uncoupling the Contributions of Hydrodynamic, Transcellular, and Paracellular Barriers. *J. Pharm. Sci.* **1995**, *84*, 1197−1204.
(31) Avdeef, A.; Artursson, P.; Neuhoff, S.; Lazorova, L.; Gråsjö, J.; Tavelin, S. Caco-2 Permeability of Weakly Basic Drugs Predicted with the Double-Sink PAMPA Method. *Eur. J. Pharm. Sci.* **2005**, *24*, 333−349.
(32) Wang, J.; Wolf, R. M.; Caldwell, J. W.; Kollman, P. A.; Case, D. A. Development and Testing of a General Amber Force Field. *J. Comput. Chem.* **2004**, *25*, 1157−1174.
(33) Vanommeslaeghe, K.; Hatcher, E.; Acharya, C.; Kundu, S.; Zhong, S.; Shim, J.; Darian, E.; Guvench, O.; Lopes, P.; Vorobyov, I.; MacKerell, A. D. CHARMM General Force Field: A Force Field for Drug-like Molecules Compatible with the CHARMM All-atom Additive Biological Force Fields. *J. Comput. Chem.* **2010**, *31*, 671−690.
(34) MacKerell, A. D., Jr.; Bashford, D.; Bellott, M.; Dunbrack, R. L., Jr.; Evanseck, J. D.; Field, M. J.; Fischer, S.; Gao, J.; Guo, H.; Ha, S.; Joseph-McCarthy, D.; Kuchnir, L.; Kuczera, K.; Lau, F. T. K.; Mattos, C.; Michnick, S.; Ngo, T.; Nguyen, D. T.; Prodhom, B.; Reiher, W. E., III; Roux, B.; Schlenkrich, M.; Smith, J. C.; Stote, R.; Straub, J.; Watanabe, M.; Wiórkiewicz-Kuczera, J.; Yin, D.; Karplus, M. All−atom Empirical Potential for Molecular Modeling and Dynamics Studies of Proteins. *J. Phys. Chem. B* **1998**, *102*, 3586−3616.
(35) Cornell, W. D.; Cieplak, P.; Bayly, C. I.; Gould, I. R.; Merz, K. M.; Ferguson, D. M.; Spellmeyer, D. C.; Fox, T.; Caldwell, J. W.; Kollman, P. A. A Second Generation Force Field for the Simulation of Proteins, Nucleic Acids, and Organic Molecules. *J. Am. Chem. Soc.* **1995**, *117*, 5179−5197.
(36) Jorgensen, W. L.; Maxwell, D. S.; Tirado-Rives, J. Development and Testing of the OPLS All-Atom Force Field on Conformati Onal Energetics and Properties of Organic Liquids. *J. Am. Chem. Soc.* **1996**, *118*, 11225−11236.
(37) Oostenbrink, C.; Villa, A.; Mark, A.; Van Gunsteren, W. A Biomolecular Force Field Based on the Free Enthalpy of Hydration and Solvation: The GROMOS Force-field Parameter Sets 53A5 and 53A6. *J. Comput. Chem.* **2004**, *25*, 1656−1676.
(38) Aksimentiev, A.; Schulten, K. Imaging α−hemolysin with Molecular Dynamics: Ionic Conductance, Osmotic Permeability, and the Electrostatic Potential Map. *Biophys. J.* **2005**, *88*, 3745−3761.
(39) Horn, H. W.; Swope, W. C.; Pitera, J. W.; Madura, J. D.; Dick, T. J.; Hura, G. L.; Head-Gordon, T. Development of an Improved Four-site Water Model for Biomolecular Simulations: TIP4P-Ew. *J. Chem. Phys.* **2004**, *120*, 9665.
(40) Nutt, D. R.; Smith, J. C. Molecular Dynamics Simulations of Proteins: Can the Explicit Water Model Be Varied? *J. Chem. Theory Comput.* **2007**, *3*, 1550−1560.
(41) Beauchamp, K. A.; Lin, Y.-S.; Das, R.; Pande, V. S. Are Protein Force Fields Getting Better? A Systematic Benchmark on 524 Diverse NMR Measurements. *J. Chem. Theory Comput.* **2012**, *8*, 1409−1414.
(42) Klauda, J.; Venable, R.; Freites, J.; O'Connor, J.; Tobias, D.; Mondragon-Ramirez, C.; Vorobyov, I.; MacKerell, A., Jr; Pastor, R. Update of the CHARMM All-Atom Additive Force Field for Lipids: Validation on Six Lipid Types. *J. Phys. Chem. B* **2010**, *114*, 7830−7843.
(43) Klauda, J. B.; Venable, R. M.; MacKerell, A. D., Jr; Pastor, R. W. Considerations for Lipid Force Field Development. *Curr. Topics Membr.* **2008**, *60*, 1−48.
(44) Koopman, E.; Lowe, C. Advantages of a Lowe-Andersen Thermostat in Molecular Dynamics Simulations. *J. Chem. Phys.* **2006**, *124*, 204103.
(45) Darve, E.; Pohorille, A. Calculating Free Energies Using Average Force. *J. Chem. Phys.* **2001**, *115*, 9169−9183.
(46) Hénin, J.; Chipot, C. Overcoming Free Energy Barriers Using Unconstrained Molecular Dynamics Simulations. *J. Chem. Phys.* **2004**, *121*, 2904−2914.
(47) Dose, V. Bayesian Inference in Physics: Case Studies. *Rep. Prog. Phys.* **2003**, *66*, 1421.
(48) von Toussaint, U. Bayesian Inference in Surface Physics. *Rev. Mod. Phys.* **2011**, *83*, 943−999.
(49) Best, R.; Hummer, G. Diffusion Models of Protein Folding. *Phys. Chem. Chem. Phys.* **2011**, *13*, 16902−16911.
(50) Metropolis, N.; Rosenbluth, M.; Rosenbluth, A.; Teller, A.; Teller, E. Equation of State Calculations by Fast Computing Machines. *J. Chem. Phys.* **1953**, *21*, 1087−1092.
(51) Humphrey, W.; Dalke, A.; Schulten, K. VMD − Visual Molecular Dynamics. *J. Mol. Graphics* **1996**, *14*, 33−38.
(52) Phillips, J. C.; Braun, R.; Wang, W.; Gumbart, J.; Tajkhorshid, E.; Villa, E.; Chipot, C.; Skeel, R. D.; Kale, L.; Schulten, K. Scalable Molecular Dynamics with NAMD. *J. Comput. Chem.* **2005**, *26*, 1781−1802.
(53) Darden, T. A.; York, D. M.; Pedersen, L. G. Particle Mesh Ewald: An *N* log *N* Method for Ewald Sums in Large Systems. *J. Chem. Phys.* **1993**, *98*, 10089−10092.
(54) Tuckerman, M. E.; Berne, B. J.; Martyna, G. J. Reversible Multiple Time Scale Molecular Dynamics. *J. Phys. Chem. B* **1992**, *97*, 1990−2001.
(55) Miyamoto, S.; Kollman, P. A. SETTLE: An Analytical Version of the SHAKE and RATTLE Algorithm for Rigid Water Molecules. *J. Comput. Chem.* **1992**, *13*, 952−962.
(56) Andersen, H. Rattle: A "velocity" Version of the Shake Algorithm for Molecular Dynamics Calculations. *J. Comput. Phys.* **1983**, *52*, 24−34.
(57) Feller, S. E.; Zhang, Y. H.; Pastor, R. W.; Brooks, B. R. Constant Pressure Molecular Dynamics Simulations — The Langevin Piston Method. *J. Chem. Phys.* **1995**, *103*, 4613−4621.

(58) Comer, J.; Dehez, F.; Cai, W.; Chipot, C. Water Conduction Through a Peptide Nanotube. *J. Phys. Chem. C* **2013**, *117*, 26797−26803.
(59) Koenig, S. H.; Ahkong, Q. F.; Brown, R. D.; Lafleur, M.; Spiller, M.; Unger, E.; Tilcock, C. Permeability of Liposomal Membranes to Water: Results from the Magnetic Field Dependence of T1 of Solvent Protons in Suspensions of Vesicles with Entrapped Paramagnetic Ions. *Magn. Reson. Med.* **1992**, *23*, 275−286.
(60) Rodriguez-Gomez, D.; Darve, E.; Pohorille, A. Assessing the Efficiency of Free Energy Calculation Methods. *J. Chem. Phys.* **2004**, *120*, 3563.
(61) Hermans, J.; Berendsen, H. J.; Van Gunsteren, W. F.; Postma, J. P. A Consistent Empirical Potential for Water−protein Interactions. *Biopolymers* **1984**, *23*, 1513−1518.
(62) Berger, O.; Edholm, O.; Jähnig, F. Molecular Dynamics Simulations of a Fluid Bilayer of Dipalmitoylphosphatidylcholine at Full Hydration, Constant Pressure, and Constant Temperature. *Biophys. J.* **1997**, *72*, 2002−2013.
(63) Tieleman, D. P.; MacCallum, J. L.; Ash, W. L.; Kandt, C.; Xu, Z.; Monticelli, L. Membrane Protein Simulations with a United-atom Lipid and All-atom Protein Model: Lipid−protein Interactions, Side Chain Transfer Free Energies and Model Proteins. *J. Phys.: Condens. Matter* **2006**, *18*, S1221.
(64) Hénin, J.; Shinoda, W.; Klein, M. United-atom Acyl Chains for CHARMM Phospholipids. *J. Phys. Chem. B* **2008**, *112*, 7008−7015.
(65) Wohlert, J.; Edholm, O. Dynamics in Atomistic Simulations of Phospholipid Membranes: Nuclear Magnetic Resonance Relaxation Rates and Lateral Diffusion. *J. Chem. Phys.* **2006**, *125*, 204703.
(66) Falck, E.; Róg, T.; Karttunen, M.; Vattulainen, I. Lateral Diffusion in Lipid Membranes through Collective Flows. *J. Am. Chem. Soc.* **2008**, *130*, 44−45.
(67) Flenner, E.; Das, J.; Rheinstädter, M. C.; Kosztin, I. Subdiffusion and Lateral Diffusion Coefficient of Lipid Atoms and Molecules in Phospholipid Bilayers. *Phys. Rev. E* **2009**, *79*, 011907.
(68) Kou, S.; Xie, X. Generalized Langevin Equation with Fractional Gaussian Noise: Subdiffusion within a Single Protein Molecule. *Phys. Rev. Lett.* **2004**, *93*, 180603.
(69) Weiss, M.; Elsner, M.; Kartberg, F.; Nilsson, T. Anomalous Subdiffusion Is a Measure for Cytoplasmic Crowding in Living Cells. *Biophys. J.* **2004**, *87*, 3518−3524.
(70) Burnecki, K.; Kepten, E.; Janczura, J.; Bronshtein, I.; Garini, Y.; Weron, A. Universal Algorithm for Identification of Fractional Brownian Motion. A Case of Telomere Subdiffusion. *Biophys. J.* **2012**, *103*, 1839−1847.
(71) Bemporad, D.; Luttmann, C.; Essex, J. Behaviour of Small Solutes and Large Drugs in a Lipid Bilayer from Computer Simulations. *Biochim. Biophys. Acta, Biomembr.* **2005**, *1718*, 1−21.
(72) Parisio, G.; Stocchero, M.; Ferrarini, A. Passive Membrane Permeability: Beyond the Standard Solubility-Diffusion Model. *J. Chem. Theory Comput.* **2013**, *9*, 5236−5246.